Contribution from the Laboratorium für Anorganische Chemie der Eidgenössischen Technischen Hochschule, ETH Zentrum, Universitätsstrasse 6, CH-8092 Zürich, Switzerland, Istituto di Chimica Farmaceutica dell'Universita di Milano, Viale Abruzzi 42, I-20131 Milano, Italy, and Inorganic Chemistry Laboratory, University of Oxford, South Parks Road, Oxford OX1 3QR, U.K.

A New Class of Planar Mixed Metal Clusters Containing a $[Pt_3(CO)_3(PR_3)_3]$ Moiety Capped by Two HgX Units

Alberto Albinati,[†] Klaus-Hermann Dahmen,[‡] Francesco Demartin,[†] Jennifer M. Forward,[§] Cindy J. Longley,[‡] D. Michael P. Mingos,*[,§] and Luigi M. Venanzi*[,‡]

Received September 5, 1991

The reaction of the clusters $[Pt_3(\mu_2\text{-}CO)_3L_3]$ (L = PCy_3, $PPhCy_2$, PPh^iPr_2, and P^iPr_3) with mercury halides (Hg_2X_2 and HgX_2) gave trigonal-bipyramidal pentametallic clusters of the type $[\{HgX\}_2\{Pt_3(\mu_2\text{-}CO)_3L_3\}]$ which were fully characterized by multinuclear NMR. While these clusters are monomeric in solution, the X-ray crystal structure of $[\{HgBr\}_2\{Pt_3(\mu_2\text{-}CO)_3(PPhCy_2)_3\}]$ shows that this compound is dimeric in the solid state and consists of two Hg_2Pt_3 trigonal bipyramids, each being bonded to a bromine atom on one side and two bridging bromine atoms on the other side. Crystal data are as follows: trigonal space group $R\bar{3}c$ (No. 167), a = 21.232 (3) Å, c = 58.494 (9) Å, V = 22836 (3) Å^3, and Z = 6. The structure was refined to R = 0.038 (R_w = 0.044) for 1294 data with $I \geq 3.0(I)$.

Introduction

Heterometallic transition-metal clusters have received considerable attention in both homogeneous and heterogeneous catalysis.[1a] Cluster compounds catalyze reactions such as hydrogenation of carbon monoxide and alkenes[1a,b] or the water–gas shift reaction.[1a,b] Furthermore, it is expected that their study will provide a better understanding of metal–metal bonding.[1c] Therefore, one is interested in finding a systematic methodology of preparing both homometallic and heterometallic clusters.

A frequently recurring feature of cluster compounds is the appearance of basic "building blocks".[2] One particularly versatile block is $[Pt_3(\mu_2\text{-}CO)_3L_3]$ (L = tertiary phosphine),[3] probably because this unit possesses HOMO and LUMO molecular orbitals which have σ-donor and weak π-acceptor properties similar to those of monodentate phosphine ligands (see later).[4] Thus the $[Pt_3(\mu_2\text{-}CO)_3L_3]$ units form two main classes of heterometallic clusters, one of "sandwich type", $[M\{Pt_3(\mu_2\text{-}CO)_3L_3\}_2]^+$ (M = Cu (**1**),[5] M = Ag (**2**),[6] M = Au (**3**)[7]) and the other of "half-sandwich type", $[\{ML\}\{Pt_3(\mu_2\text{-}CO)_3L_3\}]^+$ (M = Cu (**4**),[5] M = Ag (**5**),[5] M = Au (**6**)[8]). Furthermore, the $[Pt_3(\mu_2\text{-}CO)_3L_3]$-clusters react with metallic mercury giving sandwich-type complexes of composition $[\{Hg_2\}\{Pt_3(\mu_2\text{-}CO)_3L_3\}_2]$ (**7**).[9] Finally, the $[Pt_3(\mu_2\text{-}CO)_3L_3]$ clusters react with donors such as PR_3 and CO.[10] In the former case PR_3 is added to one Pt atom giving the cluster type $[Pt_3(\mu_2\text{-}CO)_3L_4]$ while in the latter case a rearrangement of the Pt_3 cluster unit occurs with formation of tetrametallic compounds of the type $[Pt_4(\mu_2\text{-}CO)_5L_4]$.

However, to our knowledge, no cluster is known in which the $[Pt_3(\mu_2\text{-}CO)_3L_3]$ unit is capped by a metal center on both sides. We report here the synthesis of a class of compounds of this type, i.e., $[\{HgX\}_2\{Pt_3(\mu_2\text{-}CO)_3L_3\}]$, and the X-ray crystal structure of one of them, i.e., $[\{HgBr\}_2\{Pt_3(\mu_2\text{-}CO)_3(PPhCy_2)_3\}]$.

Results and Discussion

Synthesis. Compounds of the type $[\{HgX\}_2\{Pt_3(\mu_2\text{-}CO)_3L_3\}]$ (L = PCy_3 (**8**), L = $PPhCy_2$ (**9**), L = PPh^iPr_2 (**10**), L = P^iPr_3 (**11**); a = Cl, b = Br, c = I) can easily be prepared by reacting dichloromethane or benzene solutions of compounds of the type $[Pt_3(\mu_2\text{-}CO)_3L_3]$ (L = PCy_3 (**12**), L = $PPhCy_2$ (**13**), L = PPh^iPr_2 (**14**), L = P^iPr_3 (**15**)) with mercury(I) halides (eq 1). $^{31}P\{^1H\}$ NMR studies show that this reaction is quantitative.

$$\underset{\mathbf{12-15}}{[Pt_3(\mu_2\text{-}CO)_3L_3]} + Hg_2X_2 \rightarrow \underset{\mathbf{8-11}}{[\{HgX\}_2\{Pt_3(\mu_2\text{-}CO)_3L_3\}]} \quad (1)$$

The same products can be prepared by reacting the Pt_3 clusters $[Pt_3(\mu_2\text{-}CO)_3L_3]$ (**12–15**) with HgX_2. However, in these cases, platinum(I)- and platinum(II)-containing species are also formed. This behavior is exemplified by the reaction of $[Pt_3(\mu_2\text{-}CO)_3(PPh^iPr_2)_3]$ (**14**) with HgI_2. $^{31}P\{^1H\}$ and $^{195}Pt\{^1H\}$ NMR studies show the formation of an isomeric mixture of *cis*- and *trans*-$[PtI_2(CO)(PPh^iPr_2)]$ (**16**) and of $[Pt_2I_2(CO)_2(PPh^iPr_2)_2]$ (**17**) in addition to the Hg cluster **10c**. The ratio of the oxidized platinum species **16** and **17** depends on the relative amounts of the Pt_3 cluster **14** and HgI_2 used. When these are reacted in the ratio Pt_3:HgI_2 > 1, the solution contains unreacted starting material **14**, the mercury halide cluster **10c**, and the Pt(I) compound **17**. However, when the reactant ratio Pt_3:HgI_2 is 3:4, the relative amounts of the cluster **10c** and the Pt species **16** and **17** are formed as are shown in eq 2. When the reactant ratio is 1.33:2, one obtains

$$\underset{\mathbf{14}}{3[Pt_3(\mu_2\text{-}CO)_3(PPh^iPr_2)_3]} + 4HgI_2 \rightarrow \underset{\mathbf{10c}}{2[\{HgI\}_2\{Pt_3(\mu_2\text{-}CO)_3(PPh^iPr_2)_3\}]} + \underset{\mathbf{17}}{[Pt_2I_2(CO)_2(PPh^iPr_2)_2]} + \underset{\mathbf{16}}{[PtI_2(CO)(PPh^iPr_2)]} \quad (2)$$

only equivalent amounts of **10c** and **16** (eq 3). The presence of

$$\underset{\mathbf{14}}{\tfrac{4}{3}[Pt_3(\mu_2\text{-}CO)_3(PPh^iPr_2)_3]} + 2HgI_2 \rightarrow \underset{\mathbf{10c}}{[\{HgI\}_2\{Pt_3(\mu_2\text{-}CO)_3(PPh^iPr_2)_3\}]} + \underset{\mathbf{16}}{[PtI_2(CO)(PPh^iPr_2)]} \quad (3)$$

16 and **17** was demonstrated by comparing their NMR parameters with those of the same species prepared independently by oxidizing $[Pt_3(\mu_2\text{-}CO)_3(PPh^iPr_2)_3]$ (**14**) with I_2.[11] Thus, the reaction of $[Pt_3(\mu_2\text{-}CO)_3L_3]$ with HgI_2 can then be described as redox reaction, where a part of the platinum(0) cluster is first oxidized to Pt(I) and then to Pt(II), while Hg(II) is reduced to Hg(I).

The mercury halide cluster **10c** was also obtained by I_2 oxidation of the mercury cluster $[\{Hg_2\}\{Pt_3(\mu_2\text{-}CO)_3(PPh^iPr_2)_3\}_2]$ (**7a**), as

[†] Università di Milano.
[‡] Eidgenössische Technische Hochschule Zürich.
[§] University of Oxford.

(1) (a) Braunstein, P.; Rose, J. In *Stereochemistry of Organometallic and Inorganic Compounds*; Bernal, I., Ed.; Elsevier: Amsterdam, 1989; Vol. 3. (b) Clark, H. C.; Jain, V. K. *Coord. Chem. Rev.* **1984**, *55*, 151. (c) Muetterties, E. L.; Rhodin, T. N.; Band, E.; Brucker, C. F.; Pretzer, W. R. *Chem. Rev.* **1979**, *79*, 91.
(2) Braunstein, P. *Nouv. J. Chim.* **1986**, *10*, 365.
(3) Barbier, J. P.; Bender, R.; Braunstein, P.; Fischer, J.; Ricard, L. *J. Chem. Res. Synop.* **1978**, 2913; *J. Chem. Res. Miniprint* **1978**, 2913.
(4) Gilmour, D. I.; Mingos, D. M. P. *J. Organomet. Chem.* **1986**, *302*, 127.
(5) Dahmen, K.-H. Ph.D. Thesis ETH Zürich N. 8172, 1986.
(6) Albinati, A.; Dahmen, K.-H.; Togni, A.; Venanzi, L. M. *Angew. Chem.* **1985**, *97*, 760.
(7) Hallam, M. F.; Mingos, D. M. P.; Adatia, T.; McPartlin, M. *J. Chem. Soc., Dalton Trans.* **1987**, 335.
(8) Briant, C. E.; Wardle, R. W. M.; Mingos, D. M. P. *J. Organomet. Chem.* **1984**, *C49*, 267.
(9) Albinati, A.; Moor, A.; Pregosin, P. S.; Venanzi, L. M. *J. Am. Chem. Soc.* **1982**, *104*, 7672.
(10) (a) Chatt, J.; Chini, P. *J. Chem. Soc. A* **1970**, 1538. (b) Bender, R.; Braunstein, P.; Fischer, J.; Ricard, L.; Mitschler, A. *Nouv. J. Chem.* **1981**, *5*, 81 (see Note 8).
(11) Goel, A.; Goel, S. *Inorg. Nucl. Chem. Lett.* **1980**, *16*, 317.

0020-1669/92/1331-2223$03.00/0

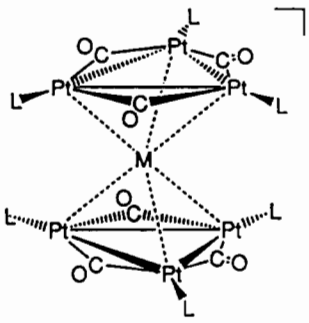

1–3

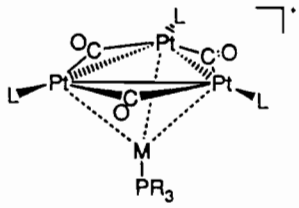

4–6

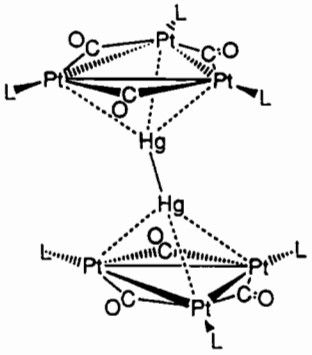

7

Table I. ^{31}P and ^{195}Pt NMR Data of the Clusters $[\{HgX\}_2\{Pt_3(\mu_2\text{-}CO)_3L_3\}]$[a]

	phosphine	X	$\delta(^{31}P)$	$\delta(^{195}Pt)$	$^1J(Pt,P)$, Hz	$^2J(Pt,P)$, Hz	$^3J(P,P)$, Hz	$^1J(Pt,Pt)$, Hz	$^2J(Hg,P)$, Hz	$^1J(Hg,Pt)$, Hz
8a	PCy_3	Cl	60.7	*c*	5083	140	38	*c*	240	*c*
8b		Br	60.5	−4168	5064	140	39	1620	229	6670
8c		I	60.5	−4121	5031	150	39	1700	190	5784
9a	$PPhCy_2$	Cl	60.3	−4247	5327	162	38	1609	244	7177
9b		Br	60.3	−4218	5319	164	38	1620	230	6723
9c		I	60.7	−4182	5293	174	39	1800	214	
10b	PPh^iPr_2	Br	69.0	*b*	5314	167	38	1750	286	*b*
10c		I	68.8	−4210	5283	177	39	1860	219	6018
11b	P^iPr_3	Br	70.9	*b*	5073	143	39	1709	220	*b*
11c		I	69.3	*b*	5050	150	39	*c*	189	*c*

[a] Measured at room temperature in C_6D_6. [b] Not measured. [c] Not detectable because of the low solubility of the cluster.

shown by a ^{31}P NMR study of this reaction (eq 4). However, compound **10c** thus produced was contaminated with unidentified decomposition products. The reaction of $[\{Hg_2\}\{Pt_3(\mu_2\text{-}CO)_3(PPh^iPr_2)_3\}_2]$ (**7a**) + I_2 → $[\{HgI\}_2\{Pt_3(\mu_2\text{-}CO)_3(PPh^iPr_2)_3\}]$ (**10c**) + ... (4)

$(PCy_3)_3\}_2]$ (**7b**) with CH_2Cl_2, as well as the reaction of $[Pt_3(\mu_2\text{-}CO)_3(PCy)_3]$ (**12**) with metallic mercury in CH_2Cl_2 also gave the mercury chloride cluster $[\{HgCl\}_2[Pt_3(\mu_2\text{-}CO)_3(PCy_3)_3]]$ (**8a**). However, during these reactions also some Pt(II) compounds were also formed.

The yields of the products were high (60–80%) when Hg_2X_2 was used, whereas they were much lower (30%) when HgX_2 was employed. Molecular weight determinations indicated that the complexes **8–11** are monomeric in solution.

IR studies of $[\{HgX\}_2\{Pt_3(\mu_2\text{-}CO)_3L_3\}]$ show the same pattern of carbonyl stretching frequencies as found for the corresponding $[Pt_3(\mu_2\text{-}CO)_3L_3]$ species (see Experimental Section) indicating that in the solid mercury complexes the Pt_3 block is retained.

$^{31}P\{^1H\}$ and $^{195}Pt\{^1H\}$ NMR Studies. ^{31}P and ^{195}Pt NMR spectroscopic studies have proved to be particularly useful for the characterization and identification of platinum carbonyl phosphine clusters of the type $[Pt_3(\mu_2\text{-}CO)_3(PR_3)_3]$, $[Pt_3(\mu_2\text{-}CO)_3(PR_3)_4]$, and $[Pt_4(\mu_2\text{-}CO)_5(PR_3)_4]$ as each of them shows a characteristic resonance pattern.[12,13] These patterns are mainly due to the NMR-active ^{195}Pt isotope ($I = {}^1/_2$, natural abundance 33.7%) bonded to the ^{31}P nuclei ($I = {}^1/_2$, natural abundance 100%). The various combinations of NMR-active and -inactive Pt isotopes give rise to different isotopomers, each with its typical spectrum.

The ^{31}P and ^{195}Pt NMR spectra of compounds **8–11** could be satisfactorily assigned on the basis of a trigonal-bipyramidal metal framework, i.e., the equilateral Pt_3 triangle capped by two mercury atoms sketched in Scheme I. The different isotopomers of these clusters are also shown in Scheme I. These take into account also the presence of the ^{199}Hg isotope ($I = {}^1/_2$, natural abundance 16.84%).

Scheme I. Abundance of Isotopomers and Spin System in $[Pt_3(\mu_2\text{-}CO)_3(PR_3)_3]$ and $[\{HgX\}_2\{Pt_3(\mu_2\text{-}CO)_3(PR_3)_3\}]$ (Circled Nuclei = ^{195}Pt and ^{199}Hg)

		I	II	III	IV
		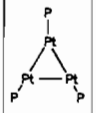	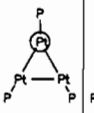	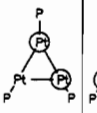	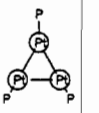
		29.63%	44.44%	22.22%	3.70%
		A_3	$A_2A'X$	$AA'A''XX'$	$AA'A''XX''X''$
a	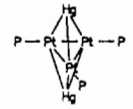	20.49%	30.73%	15.36%	2.55%
		A_3	$A_2A'X$	$AA'A''XX'$	$AA'A''XX''X''$
b	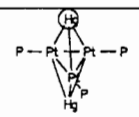	8.29%	12.45%	6.22%	1.04%
		A_3B	$A_2A'BX$	$AA'A''BXX'$	$AA'A''BXX''X''$
c	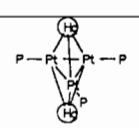	0.84%	1.26%	0.63%	0.105%
		A_3B_2	A_2AB_2X'	$AA'A''B_2XX'$	$AA'A''B_2XX''X''$

The $^{31}P\{^1H\}$ and $^{195}Pt\{^1H\}$ NMR data of $[\{HgX\}_2\{Pt_3(\mu_2\text{-}CO)_3L_3\}]$ are summarized in Table I. The basic patterns of the spectra are similar to those shown by the $[Pt_3(\mu_2\text{-}CO)_3L_3]$ compounds. However, as mentioned earlier, additional couplings due to ^{199}Hg are observed. Both the $^{31}P\{^1H\}$ and $^{195}Pt\{^1H\}$ resonances are consistent with a structure in which the two Hg atoms are equivalent and bound to the Pt_3 triangle in such a way as to

(12) Moor, A.; Pregosin, P. S.; Venanzi, L. M. *Chim. Acta* **1981**, *48*, 153.
(13) Moor, A. Ph.D. Thesis ETH Zürich N. 7176, 1982.

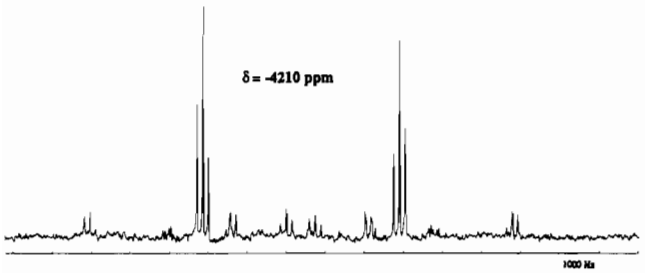

Figure 1. $^{195}Pt\{^1H\}$ NMR of $[\{HgI\}_2\{Pt_3(\mu_2\text{-}CO)_3(PPh^iPr_2)_3\}]$ (**10c**) in C_6D_6, 250 MHz, room temperature, δ = −4210 ppm.

Table II. $\Delta^1J(Pt,P)$ Values[a] (Hz) for Clusters of the Types $[\{HgX\}_2\{Pt_3(\mu_2\text{-}CO)_3L_3\}]$ and $[\{Hg\}\{Pt_3(\mu_2\text{-}CO)_3L_3\}]$[b]

L	PCy_3	$PPhCy_2$	PPh^iPr_2	P^iPr_3	ref
$[\{HgCl\}_2\{Pt_3(\mu_2\text{-}CO)_3L_3\}]$	679	703	n.r.[c]	n.r.	5
$[\{HgBr\}_2\{Pt_3(\mu_2\text{-}CO)_3L_3\}]$	660	695	713	648	6
$[\{HgI\}_2\{Pt_3(\mu_2\text{-}CO)_3L_3\}]$	618	670	680	638	5
$[\{Hg\}\{Pt_3(\mu_2\text{-}CO)_3L_3\}]$	155	142	180	221	5, 13

[a] Defined as $(^1J(Pt,P)_{Hg_2Pt_3\text{-cluster}} - {}^1J(Pt,P)_{Pt_3\text{-cluster}})$. [b] The following $^1J(Pt,P)$ values (Hz) were used: L = PCy_3, 4412; L = $PPhCy_2$, 4622; L = PPh^iPr_2, 4605; L = P^iPr_3, 4425. [c] Not recorded.

preserve its C_3 symmetry. Although isotopomer IIb occurs with a high abundance (12.45%), its ^{31}P NMR spectrum cannot be observed as this $A_2A'BX$ spin system gives rise to an 18-line pattern because of coupling with the ^{199}Hg nucleus.

Mercury–phosphorus couplings can only be observed in the ^{31}P NMR resonances due to the subspectrum of the isotopomer Ib, an A_3B spin system, with an abundance of 8.28%. The $^{195}Pt\{^1H\}$ NMR spectrum is clearly dominated by the subspectrum due to isotopomer IIb, and therefore coupling between Hg and Pt is directly detectable (see Figure 1).

The $^{31}P\{^1H\}$ NMR spectra of these complexes unambiguously show that two equivalent Hg atoms are linked to the Pt_3 cluster. This is best seen by considering the integral ratio of the subspectrum due to isotopomer Ib, which can be easily identified in the experimental spectrum. The main feature of this subspectrum is the pseudotriplet arising from the main P resonance and coupling with the single ^{199}Hg atom. The experimental values of the integral ratio for this pseudotriplet are 4:21:4, while the calculated ratio is 4.14:20.49:4.14. However, the intensity of the central resonance must be corrected for the contribution due to the central signal of isotopomer Ic, which is a 1:2:1 triplet. The calculated intensity of its central line is 0.42% of the calculated intensity of the central line of the subspectrum due to Ib. Therefore, the total calculated intensity ratio is 4.14:20.91:4.14.

The ^{31}P chemical shifts of all the mercury halide clusters of the type $[\{HgX\}_2\{Pt_3(\mu_2\text{-}CO)_3L_3\}]$ are slightly shifted toward high field relative to $[Pt_3(\mu_2\text{-}CO)_3L_3]$. However, the coordination chemical shift[14] Δ ($\Delta = \delta_{complex} - \delta_{free}$) for all platinum carbonyl phosphine clusters remains 60 ± 10 Hz, indicating that all these compounds have similar structure and bonding.

The ^{195}Pt chemical shifts of the mercury clusters range from −4121 to −4247 ppm; i.e., they are shifted upfield relative to the parent Pt_3 clusters (−4392 to −4450 ppm).[5]

The change in the electronic structure of the $[Pt_3(\mu_2\text{-}CO)_3L_3]$ unit caused by "addition" of other metal fragments is clearly shown by comparing the $\Delta^1J(Pt,P)$ values (defined as $^1J(Pt,P)_{Hg_2Pt_3\text{-cluster}} - {}^1J(Pt,P)_{Pt_3\text{-cluster}}$). These values for the various classes of clusters are listed in Table II. As can be seen there, those for the mercury halide clusters **8–11** are in the range 618–713 Hz while those of the $[\{Hg\}_2\{Pt_3(\mu_2\text{-}CO)_3L_3\}_2]$ clusters are in the range 142–221 Hz.

Furthermore, the $^1J(Pt,P)$ values of the Pt_3 clusters, as well as those derived from them, are an approximately linear function of Tolman's "electronic parameter", ν, defined as $\nu = \nu_{CO}(A_1)$ in $[Ni(CO)_3L]$.[14] This relationship is shown in Figure 2. As can be seen there, a decrease in basicity of the phosphine causes an increase in the $^1J(Pt,P)$ value.

(14) Tolman, C. A. *Chem. Rev.* **1977**, *77*, 313.

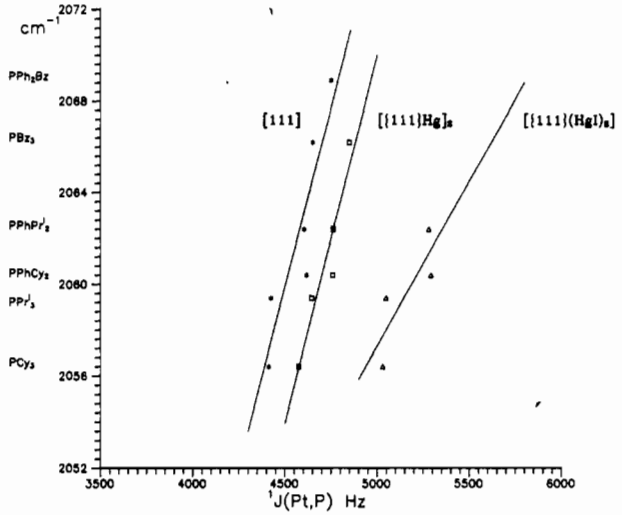

Figure 2. Phosphine dependence of the $^1J(Pt,P)$ values for clusters of the type $[Pt_3(\mu_2\text{-}CO)_3(PR)_3]$, $[\{HgI\}_2\{Pt_3(\mu_2\text{-}CO)_3(PR_3)_3\}]$, and $[Hg\{Pt_3(\mu_2\text{-}CO)_3(PR)_3\}]_2$.

Table III. Selected Bond Lengths (Å) and Angles (deg) for $[\{HgBr\}_2\{Pt_3(\mu_2\text{-}CO)_3(PPhCy_2)_3\}\{\mu\text{-}HgBr\}_2]$ $\{\mathbf{9b}\}_2$

Hg(1)–Pt	2.834 (1)	Pt–Hg(1)–Br(1)	147.24 (2)
Hg(1)–Br(1)	2.494 (5)[a]	Pt–Hg(1)–Pt'[d]	55.90 (4)
Hg(2)–Pt	2.853 (1)	Pt–Hg(2)–Pt'	55.49 (4)
Hg(2)–Br(2)	2.709 (11)[b]	Pt–Hg(2)–Br(2)	117.7 (2)
Hg(2')–Br(2)	2.728 (2)[c]	Hg(1)–Pt–Hg(2)	114.72 (3)
Pt–Pt	2.656 (1)	Hg(1)–Pt–Pt'	62.05 (2)
Pt–P	2.258 (6)	Hg(1)–Pt–P	121.3 (1)
Pt–C	1.99 (2)	Hg(1)–Pt–C	83.2 (5)
Pt'–C	1.99 (2)	Hg(2)–Pt–Pt'	62.26 (2)
C–O	1.26 (2)	Pt'–Pt–C	48.3 (5)
		Pt–C–Pt	83.8 (8)
		Pt–C–O	138.8 (1.5)
		Pt–Pt–P	150.6 (1)
		Hg(2)–Br(2)–Hg(2'')	95.0 (2)
		Br(2)–Hg–Br(2')	82.6 (3)[a]

[a–c] The corresponding values in $[Hg_2Br_2(\mu\text{-}Br)_2$ ((diphenylphosphino)acetic acid)$_2]$ (**18b**) are 2.519 (1), 2.726 (1), and 2.811 (1) Å, respectively.[15] [d] The primed atoms are related to those unprimed by the symmetry operation: $\bar{y}, x-y, z$; $\bar{x}, y-x, {}^1/_2 - z$. [e] The corresponding value in **18b** is 89.0 (1)°.

The X-ray Crystal Structure of $[\{HgBr\}_2\{Pt_3(\mu_2\text{-}CO)_3(PPhCy_2)_3\}_2\{\mu\text{-}HgBr\}_2]$, $\{\mathbf{9b}\}_2$. A selection of bond lengths and angles is given in Table III and a full list is given in Supplemental Table S4. An ORTEP view of the full molecule is shown in Figure 3 (the numbering scheme is shown in Supplemental Figure 1). As can be more clearly seen in Figure 4, which shows the cluster core, compound **9b**, *although monomeric in solution*, is present as a bromine-bridged dimer $\{\mathbf{9b}\}_2$ in the solid state.

The central part of the cluster core consists of a square-planar arrangement of two mercury atoms and two bridging bromine atoms. In addition, each of these mercury atoms is bonded to the triangular Pt_3 unit of the $[Pt_3(\mu_2\text{-}CO)_3L_3]$ cluster, the latter being capped by an Hg–Br fragment. The dimeric cluster lies on two crystallographic symmetry elements: (1) a C_3 axis going through the terminal bromine and mercury atoms, as well as the centers of the Pt_3 units; (2) a C_2 axis perpendicular to the C_3, going through the two bridging bromine atoms. Thus, the crystallographically independent atoms are Hg(1), Hg(2), Br(1), Br(2), one CO, and one phosphine. The C_3 operation gives rise to a trigonal pyramid, i.e., the top part of Figure 4, while the C_2 operation generates the bottom part of Figure 4. It also follows from the symmetry elements that the bridging bromine atoms must be disordered over six positions, only two of which are shown in Figure 4 (see Supplemental Figure S2).

There are two formal ways of looking at the molecular geometry of compound $\{\mathbf{9b}\}_2$: (1) as two trigonal-bipyramidal {**9b**} cluster units held together by Hg–Br bridges, with formation of a square

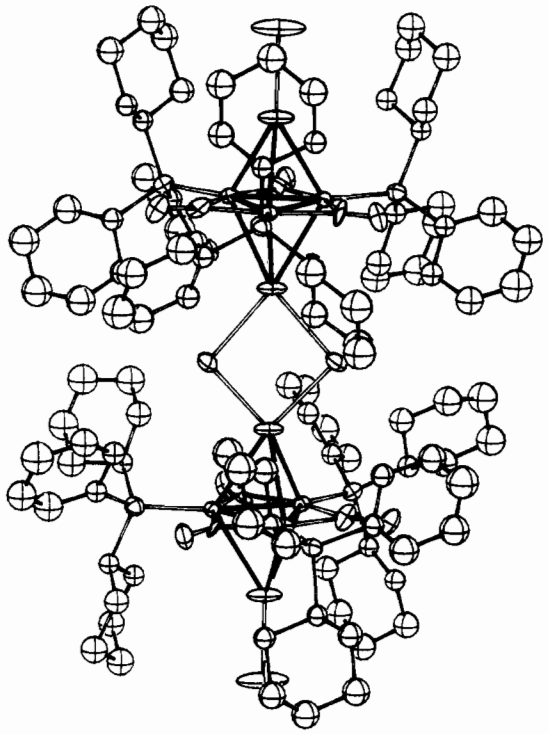

Figure 3. ORTEP view of the full molecule $[\{HgBr\}_2\{Pt_3(\mu_2\text{-}CO)_3(PPhCy_2)_3\}\{\mu\text{-}HgBr\}_2]$ ($\{\mathbf{9b}\}_2$).

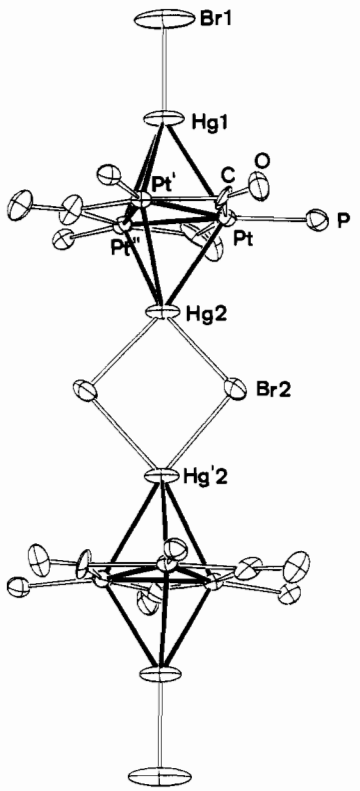

Figure 4. ORTEP view of the cluster core of $[\{HgBr\}_2\{Pt_3(\mu_2\text{-}CO)_3(PPhCy_2)_3\}\{\mu\text{-}HgBr\}_2]$ ($\{\mathbf{9b}\}_2$).

arrangement of the Hg and Br atoms; (2) as the assembly of two $\{\mu_3\text{-}HgBr\}\{Pt_3(\mu_2\text{-}CO)_3L_3\}$ units, bridged by the Hg_2Br_2 planar unit, the latter being essentially the same as that found in compounds of the type $[Hg_2X_2(\mu\text{-}X)_2L_2]$ (**18**) (L = PR_3).[15] In the latter

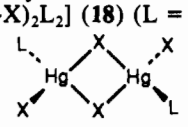

18

Table IV. Some Platinum–Metal and Platinum–Platinum Distances (Å) in Heterometallic Carbonyl Phosphine Clusters

	Pt–M	Pt–Pt	ref
$[Pt_3(\mu\text{-}CO)_3(PCy_3)_3]$ (**12**)		2.654 (2)[a]	19
$[\{HgBr\}_2\{Pt_3(\mu_2\text{-}CO)_3(PPhCy_2)_3\}]_2$ ($\{\mathbf{9b}\}_2$)	2.931 (1) 2.968 (1) 3.084 (1)	2.656 (1)[a]	*b*
$[\{Cu(P^iPr_3)\}\{Pt_3(\mu_2\text{-}CO)_3(P^iPr_3)_3\}]^+$ (**4a**)	2.585 (3) 2.593 (4) 2.633 (4)	2.671 (1)[a]	5
$[\{Au(PCy_3)\}\{Pt_3(\mu_2\text{-}CO)_3(PCy_3)_3\}]^+$ (**6a**)	2.768 (5) 2.757 (5) 2.750 (6)	2.696 (15)[a]	8
$[Cu\{Pt_3(\mu_2\text{-}CO)_3(PPh_3)_3\}_2]^+$ (**1a**)	2.605 (4) 2.598 (2) 2.598 (3)	2.650 (1)[a]	7
$[Ag\{Pt_3(\mu_2\text{-}CO)_3(PPh^iPr_2)_3\}_2]^+$ (**2a**)	2.853 (2) 2.831 (2) 2.825 (2)	2.666 (8)[a]	6
$[Au\{Pt_3(\mu_2\text{-}CO)_3(PPh_3)_3\}_2]^+$ (**3a**)	2.729 (1) 2.731 (1) 2.725 (1)	2.683 (1)[a]	7

[a] Average values. The standard deviation of the mean is given in parentheses. [b] This work.

case the halogen-bridged mercury atoms can be assigned the formal oxidation state (II), and thus the central unit can be described as $\{Hg_2X_2\}^{2+}$. The main structural features found for one compound of type **18** are also listed in Table III. As can be seen there, the bond lengths and angles of the bridging unit of $\{\mathbf{9b}\}_2$ closely resemble those of compounds of type **18**, supporting this type of formal description.

If one accepts that the $\{Hg_2Br_2\}$ core is adequately described by this formalism, it follows that each Pt_3Hg unit must be considered as being uninegative, i.e., $[\{HgBr\}\{Pt_3(\mu_2\text{-}CO)_3L_3\}]^-$. It is noteworthy that this unit is isoelectronic with the fragment $[\{Hg\}\{Pt_3(\mu_2\text{-}CO)_3L_3\}]$ found in the cluster $[\{Hg_2\}\{Pt_3(\mu_2\text{-}CO)_3L\}_2]$ (**7**),[9] which, while dimeric in the solid state, is monomeric in solution. However, the above-mentioned anion would differ from the structurally related units $[\{MPR'_3\}\{Pt_3(\mu_2\text{-}CO)_3L_3\}]^+$ (M = Cu (**4**)[5] and Au (**6**)[8]). The structural data for $\{\mathbf{9b}\}_2$, **18**, **7**, and **6** are compared in Table IV. As can be seen there, the Pt–Hg(1) distances in $\{\mathbf{9b}\}_2$ (2.834 (1) Å) are significantly shorter than the corresponding distances in **7** (these range from 2.931 (1) to 3.084 (1) Å). As the latter distances are comparable with, or larger than, the sum of the metallic radii for the two elements (2.94 Å).[16] the shorter distances in $\{\mathbf{9b}\}_2$ may reflect the higher formal oxidation state of mercury in this compound.

The Pt–Pt distances in compound $\{\mathbf{9b}\}_2$ are comparable with those observed in other heterometallic clusters containing the $[Pt_3(\mu_2\text{-}CO)_3L_3]$ unit (see Table IV). The Pt–Hg(2) distance in $\{\mathbf{9b}\}_2$ (2.853 (1) Å) is longer than the Pt–Hg(1) distances, as are the Hg(2)–X(2) distances relative to Hg(1)–X(1). This might be attributed to the higher coordination number of Hg(2) relative to that of Hg(1).

The Hg(1)–Br(1) distance (2.494 (5) Å) is comparable with the terminal Hg–Br bond in compound **18** (2.519 (1) Å) while the Hg(2)–Br(2) distance in $\{\mathbf{9b}\}_2$ is also equal to the Hg–Br(bridging) distance in compound $Hg_2Br_2(\mu\text{-}Br)_2L_2$ (L = (diphenylphosphino)acetic acid) (**18b**) (2.726 (1) Å).[15b] Similar $\{Hg_2X_2\}$ bridging units are found in compounds $[Ir_2Cl_2X_2(HgX)_2(CO)_2(PPh_3)_4]$[17] and $[Ru_3(HgBr)(CO)_3(C_6H_9)]_2$.[18] It is noteworthy that while the Hg–Br distances in the Hg_2Br_2 bridge are equal, the bridges in compounds $[Ir_2Cl_2X_2(HgX)_2(CO)_2$-

(15) (a) Bell, N. A.; Goldstein, M.; Jones, T.; Nowell, I. W. *Inorg. Chim. Acta* **1983**, *69*, 155. (b) Podlahová, J.; Kratochvíl, B.; Loub, J.; Paulus, H. *Acta Crystallogr.* **1986**, *C42*, 415.
(16) Wells, A. F. *Structural Inorganic Chemistry*; 5th ed.; Oxford University Press: Oxford, 1984; p 1288.
(17) Brotherton, P. D.; Raston, L. L.; White, A. H.; Wild, S. B. *J. Chem. Soc., Dalton Trans.* **1976**, 1799.
(18) Fahmy, R.; Rosenberg, K.; Tiripicchio, A.; Tiripicchio Camellini, M. *J. Am. Chem. Soc.* **1980**, *102*, 3626.

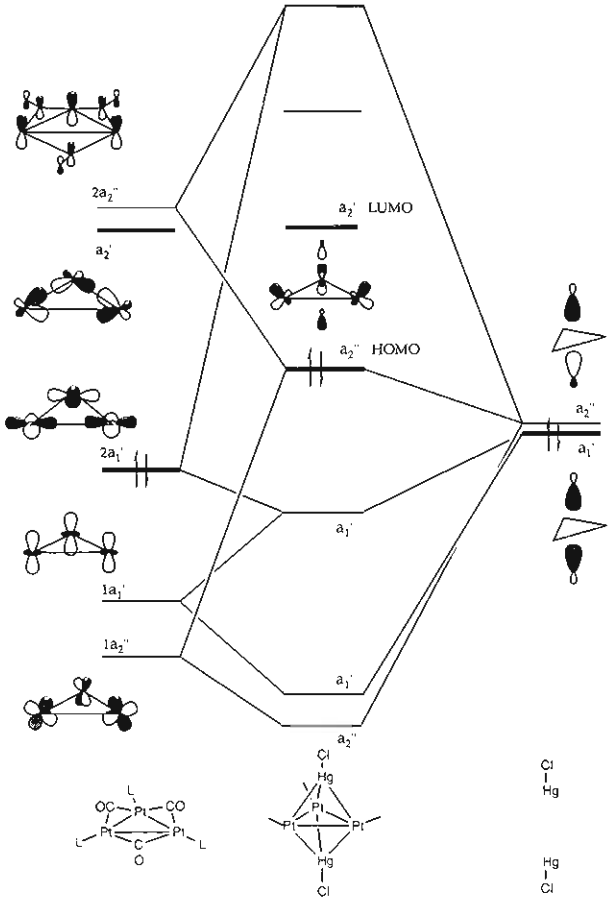

Figure 5. Molecular orbital scheme for the cluster $[\{HgCl\}\{Pt_3(\mu_2\text{-}CO)_3L_3\}\{HgCl\}]$.

$(PPh_3)_4]$[17] and $[Ru_3(HgBr)(CO)_3(C_6H_9)]_2$[18] show strong asymmetry, indicating a much weaker interaction between the two Hg–Br units of each "monomer".

Molecular Orbital Calculations. Molecular orbital calculations have been performed on both I and II. The following bond

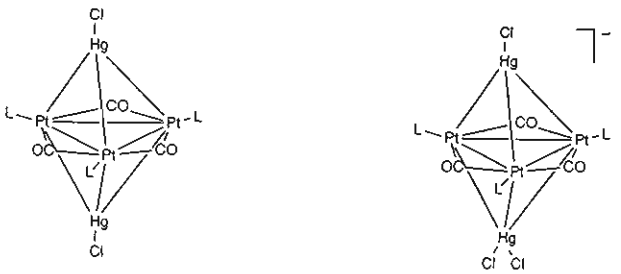

I II

distances were used: Pt–Pt, 2.70 Å; Hg–Pt, 2.85 Å; Hg–Cl, 2.650; Pt–L, 1.70 Å; Pt–C, 2.10 Å; C–O, 1.20 Å. The phosphines were modeled by a pseudoligand with an orbital exponent the same as H and an H_{ii} equal to −14.20 eV, the same as the lone pair orbital in PH_3. The other parameters used in the calculations have been given elsewhere.[4]

The bonding in the platinum triangular cluster compounds III, IV, and V has been discussed by several groups.[4,20,21] The ability

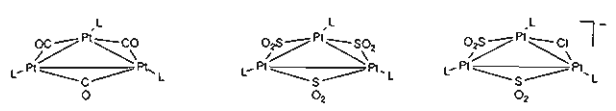

III IV V

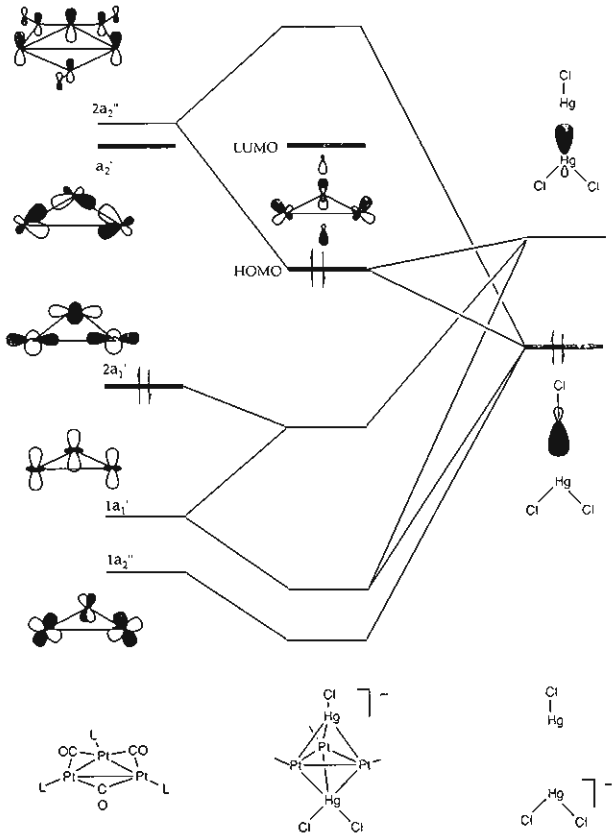

Figure 6. Molecular orbital scheme for the cluster $[\{HgCl\}\{Pt_3(\mu_2\text{-}CO)_3L_3\}\{HgCl_2\}]^-$.

of these triangular clusters to sustain 42 and 44 valence electron counts can be related to their energies and nodal characteristics. In III and IV, which have 42 electron counts, there are a pair of low lying empty molecular orbitals which have a_2' and a_2'' symmetry. These molecular orbitals are illustrated in VI and VII.

a_2' a_2''

VI VII

The bridging SO_2 and Cl ligands in V lead to a stabilization of the a_2' molecular orbital leading to the 44-electron cluster.[21]

In a previous paper we have analyzed the bonding in heterometallic clusters derived from these Pt_3 units by the introduction of d^{10} $AuPH_3^+$ capping groups.[4] The corresponding interaction diagrams for I and II are illustrated in Figures 5 and 6, respectively. The HOMO of the triangular cluster $[Pt_3(\mu_2\text{-}CO)_3L_3]$ is an orbital of a_1' symmetry which is an in-phase combination of $d_{x^2-y^2}$ platinum orbitals. The a_2' and a_2'' lowest unoccupied orbitals of the triangular cluster are displayed at the left-hand sides of the figures.

In I the in-phase a_1' combination of out-pointing orbitals on the Hg–Cl fragments interact primilarly with the HOMO of the triangle $2a_1'$ and with the lower lying $1a_1'$ orbital, which is an in-phase combination of platinum d_{z^2} orbitals. The out-of-phase combination of out-pointing Hg–Cl orbitals enters into a four-electron destabilizing interaction with $1a_2''$, which is mitigated by a bonding interaction with $2a_2''$ the latter being delocalized over the platinum atoms and the carbonyl bridges. The resulting molecular orbital is the HOMO of the cluster $[\{HgCl\}_2\{Pt_3(\mu_2\text{-}CO)_3L_3\}]$ and is shown in Figure 5. This molecular orbital is only weakly platinum–platinum and platinum–mercury bonding. It is significant that the a_2' molecular orbital of $[Pt_3(\mu_2\text{-}CO)_2L_3]$ is unaffected by the interactions involving the capping mercury atoms because of the absence of suitable a_2' molecular orbitals

(19) Albinati, A. *Inorg. Chim. Acta* **1977**, *22*, L31.
(20) Underwood, D. J.; Hoffmann, R.; Tatsumi, K.; Nakamura, A.; Yamamoto, Y. *J. Am. Chem. Soc.* **1985**, *107*, 5968.
(21) Mealli, C. *J. Am. Chem. Soc.* **1985**, *107*, 2245.

on mercury. The resultant overlap populations (IX) and charges (X) for I are summarized. In the parent Pt_3 cluster the computed Pt–Pt overlap population is 0.182.

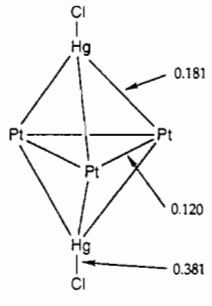

IX

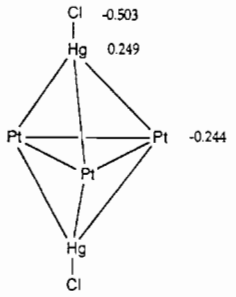

X

The bonding interactions for II are very similar to those described above, although the lower symmetry of the cluster does not permit such an easy separation of the relevant molecular orbitals. The interaction diagram is illustrated in Figure 6. On the right-hand side the out-pointing orbitals of the HgCl and $HgCl_2^-$ fragments are clearly discernible, and their interactions with the molecular orbitals of the triangle lead to a set of molecular orbitals very similar to those for I. In particular the HOMO and LUMO are almost identical. The computed overlap populations (XI) and charges (XII) summarized below are also very similar.

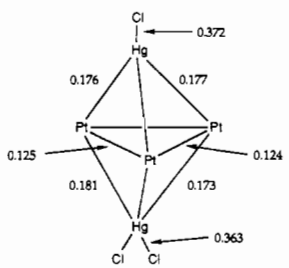

XI

XII

This calculation does not provide any clear indications of why the monomer I dimerizes in the solid state to give the structure observed in the X-ray crystallographic analysis. Certainly, the metal–metal bonding interactions in II are not stronger than those in I. It is possible that the computed positive charge on the mercury atoms in I (+0.249) would encourage nucleophilic attack from the lone pair of a halogen ligand to generate a dimer. However, all indications from the calculations are that this is a finely balanced equilibrium.

Although both $[\{Au(PAr_3)\}_2\{Pt_3(\mu_2\text{-}SO_2)_2(\mu_2\text{-}Cl)(PCy_3)_3\}]^+$ [22] and $[\{HgCl\}_2\{Pt_3(\mu_2\text{-}CO)_3(PCy_3)_3\}]$ [23] have trigonal-bipyramidal skeletal structures and are both associated with 68 valence electrons, the platinum–platinum distances are very different: in the former the average Pt–Pt distance is 2.890 Å, whereas in the latter it is 2.688 Å. We attribute this to a reversal in the HOMO and LUMO for these trigonal-bipyramidal clusters as in $[\{Au(PAr_3)\}_2\{Pt_3(\mu_2\text{-}SO_2)_2(\mu_2\text{-}Cl)(PCy_3)_3\}]^+$ the HOMO corresponds to the a_2' orbital illustrated in VI above. Since this molecular orbital is Pt–Pt antibonding, its population leads to an expansion of the platinum triangle. It is evident from Figures 5 and 6 that this orbital is not populated in the mercury trigonal-bipyramidal clusters. This difference can be attributed to the stabilizing effect on the a_2' molecular orbital of the bridging Cl and SO_2 ligands.

The bonding in the mercury clusters is very similar to that described previously for $[\{Pt_3(COD)_3\}(SnCl_3)_2]$ [24] and $[\{Ni_3(CO)_6\}\{Mo(CO)_5\}_2]^{2-}$.[25] The isolobal nature of HgCl, $SnCl_3$ and $Mo(CO)_5^-$ is responsible for these similarities, particularly since in each case the a_2'' orbital is stabilized by overlap with the out-of-phase combination of the out-pointing a_1 orbitals of these fragments.

Experimental Section

All solvents used were Fluka (puriss) and employed without further purification.

Elemental C and H analyses were carried out by the Microanalytical Service of the Organic Chemistry Laboratory of the ETH Zürich, who also carried out the molecular weight determination using vapor pressure osmometry in dichloromethane solutions. The heavy elements and their ratios were determined by the Analytical Service of the Inorganic Chemistry Laboratory of the ETH Zürich using either atomic absorption or X-ray fluorescence spectroscopy.

NMR spectra were measured using Bruker WM 250 and HX90 instruments. ^{195}Pt and ^{31}P NMR chemical shifts were calculated relative to $Na_2[PtCl_6]$ and H_3PO_4, respectively, as external standards, a positive sign indicating a chemical shift downfield of the resonance. IR spectra were reported on a Perkin-Elmer 1430 as Nujol mulls.

The compounds $[Pt_3(\mu_2\text{-}CO)_3L_3]$ (L = PCy_3, $PPhCy_2$, PPh^iPr_2, and P^iPr_3) were prepared as described elsewhere.[26]

Preparation of the Mercury Clusters. General Method. Solid Hg_2X_2 (6.63×10^{-5} mol) was added to a stirred solution of $[Pt_3(\mu_2\text{-}CO)_3L_3]$ (6.63×10^{-5} mol) in 5 mL of benzene. The solid gradually dissolved with formation of a yellowish solution which was filtered over Celite and evaporated to dryness under reduced pressure and recrystallized as described below. The color of the compounds ranges from yellow-orange to red, in the order Cl → Br → I. All the crystalline materials obtained contain solvent of crystallization which, in many cases, could not be completely removed by pumping under high vacuum. Their solubilities are moderate in solvents such as CH_2Cl_2, benzene, and toluene, slight in Et_2O, $CHCl_3$, DMF, and THF, and insoluble in MeOH, MeCN, and acetone. In general, solubilities increase in the order Cl → Br → I.

$[\{HgCl\}_2\{Pt_3(\mu_2\text{-}CO)_3(PCy_3)_3\}]\cdot C_6H_6$ (8a). The residual solid was recrystallized by dissolving it in CH_2Cl_2 followed by addition of hexane. Yield: 0.100 g (70%). IR: ν(CO) 1855 (w), 1803 (vs), 1772 (sh) cm^{-1}. Anal. Calcd for $C_{63}H_{105}O_3Cl_2Hg_2P_3Pt_3$: C, 32.92; H, 4.78. Found: C, 32.72; H, 4.84. Heavy element ratios: Calcd: P/Pt, 1.00; P/Hg, 1.50; Cl/Hg, 1.00. Found: P/Pt, 0.99 ± 0.02; P/Hg, 1.68 ± 0.06; Cl/Hg, 0.92 ± 0.05.

$[\{HgBr\}_2\{Pt_3(\mu_2\text{-}CO)_3(PCy_3)_3\}]$ (8b). The residual solid was recrystallized by leaving for ca. 12 h a sample tube, containing a benzene solution of the crude product, inside a stoppered flask containing acetone. Yield: 0.091 g (67%). IR: ν(CO) 1868 (w), 1835 (w), 1807 (vs) cm^{-1}. Anal. Calcd for $C_{57}H_{99}O_3Br_2Hg_2P_3Pt_3$: C, 33.05; H, 4.78. Found: C, 33.11; H, 4.75. Heavy element ratios: Calcd: P/Pt, 1.00; P/Hg, 1.50; Br/Hg, 1.00. Found: P/Pt, 1.10 ± 0.17; P/Hg, 1.69 ± 0.13; Br/Hg, 1.79 ± 0.22.

$[\{HgI\}_2\{Pt_3(\mu_2\text{-}CO)_3(PCy_3)_3\}]\cdot C_6H_6$ (8c). The brown solid was recrystallized by dissolving it in benzene followed by addition of hexane: yield, 0.075 g (52%); mp 195 °C (dec). IR: ν(CO) 1863 (w), 1808 (vs), 1797 (vs) cm^{-1}. Anal. Calcd for $C_{63}H_{105}O_3Hg_2I_2P_3Pt_3$: C, 33.72; H, 4.68; I, 11.33. Found: C, 33.73; H, 4.70; I, 10.58. Heavy elemental ratios: Calcd: P/Pt, 1.00; P/Hg, 1.50; I/Hg, 1.00. Found: P/Pt, 0.97 ± 0.12; P/Hg, 1.70 ± 0.03; I/Hg, 0.97 ± 0.14.

$[\{HgCl\}_2\{Pt_3(\mu_2\text{-}CO)_3(PPhCy_2)_3\}]$ (9a). The crude product was recrystallized by leaving overnight a solution in CH_2Cl_2 placed in a sample tube inside a stoppered flask containing acetone. Yield: 0.085 g (65%). IR: ν(CO) 1889 (w), 1835 (vs), 1818 (vs) cm^{-1}. Anal. Calcd for $C_{57}H_{81}O_3Cl_2Hg_2P_3Pt_3$: C, 34.88; H, 4.13; mol wt, 1962. Found: C, 34.61; H, 4.22; mol wt, 2024. Heavy element ratios: Calcd: P/Pt, 1.00; P/Hg, 1.50; Cl/Hg, 1.00. Found: P/Pt, 0.98 ± 0.02; P/Hg, 1.54 ± 0.22; Cl/Hg, 0.92 ± 0.06.

$[\{HgBr\}_2\{Pt_3(\mu_2\text{-}CO)_3(PPhCy_2)_3\}]$ (9b). Well-formed red crystals were obtained by leaving for several hours a sample tube containing a solution of the crude product in CH_2Cl_2 inside a stoppered flask containing acetone: yield, 0.112 g (82%); mp 190 °C (dec). IR: ν(CO) 1887 (w), 1832 (vs), 1814 (vs) cm^{-1}. Anal. Calcd for $C_{57}H_{81}O_3Br_2Hg_2P_3Pt_3$: C, 33.34; H, 3.94; mol wt, 2051. Found: C, 32.61; H, 4.02; mol wt, 2144. Heavy element ratios: Calcd: P/Pt, 1.00; P/Hg, 1.50; Cl/Hg, 1.00. Found: P/Pt, 0.98 ± 0.06; P/Hg, 1.69 ± 0.11; Br/Hg, 1.28 ± 0.11.

$[\{HgI\}_2\{Pt_3(\mu_2\text{-}CO)_3(PPhCy_2)_3\}]\cdot C_6H_6$ (9c). It was purified as described for **8c**. Yield: 0.115 g (81%). IR: ν(CO) 1884 (w), 1830 (vs), 1811 (vs) cm^{-1}. Anal. Calcd for $C_{63}H_{87}O_3Hg_2I_2P_3Pt_3$: C, 34.00; H, 3.91. Found: C, 33.75; H, 3.90. Heavy elemental ratios: Calcd: P/Pt, 1.00; P/Hg, 1.50; Cl/Hg, 1.00. Found: P/Pt, 0.97 ± 0.03; P/Hg, 1.71 ± 0.03; Cl/Hg, 1.00 ± 0.10.

(22) Bott, S. G.; Hallam, M. F.; Ezomo, O. J.; Mingos, D. M. P.; Williams, I. D. *J. Chem. Soc., Dalton Trans.* **1988**, 1461.
(23) Forward, J. M.; Mingos, D. M. P. Unpublished results.
(24) Guggenberger, L. J. *J. Chem. Soc., Chem. Commun.* **1968**, 512.
(25) Ruff, J. K.; White, R. P.; Dahl, L. F. *J. Am. Chem. Soc.* **1971**, *93*, 2159.
(26) Dahmen, K.-H.; Naegeli, R.; Venanzi, L. M. *Inorg. Chem.* **1991**, *30*, 4285.

Table V. Crystallographic Data and Data Collection Paramters for $\{9b\}_2 \cdot 6Me_2CO$

formula	$C_{132}H_{198}Br_4Hg_4O_{12}P_6Pt_6$
fw	4455.33
cryst syst	trigonal
space group	$R\bar{3}c$ (No. 167)
T, °C	22
a, Å	21.232 (3)
c, Å	58.494 (9)
V, Å^3	22836 (3)
Z	6
ρ_{calcd}, g cm^{-3}	1.873
λ,[a] Å	0.71069
μ, cm^{-1}	107.17
transmission coeff	0.996–0.648
R[b]	0.038
R_w[b]	0.044

[a] Graphite monochromated MoK$\bar{\alpha}$ radiation. [b] For the observed reflections: $R = \sum(|F_o| - 1/k|F_c|)/\sum|F_o|$; $R_w = [\sum w(|F_o| - 1/k|F_c|)^2/\sum w|F_o|^2]^{1/2}$ where $w = [\sigma^2(F_o)]^{-1}$ and $\sigma(F_o) = [\sigma^2(I) + f^2(F_o^2)^2]^{1/2}/2F_o$ with $f = 0.06$.

$[\{HgBr\}_2\{Pt_3(\mu_2\text{-}CO)_3(PPh^iPr_2)_3\}]$ (10b). It was not isolated. The purity of the product was checked by $^{31}P\{^1H\}$ NMR spectroscopy.

$[\{HgI\}_2\{Pt_3(\mu_2\text{-}CO)_3(PPh^iPr_2)_3\}]\cdot C_6H_6$ (10c). The crude product was recrystallized by adding hexane to a benzene solution until incipient precipitation and storing the flask at 8 °C: yield, 0.085 g (65%); mp 175 °C. IR: ν(CO) 1810 (vs), 1830 (vs), 1880 (w) cm^{-1}. Anal. Calcd for $C_{45}H_{63}O_3Hg_2I_2P_3Pt_3$: C, 27.25; H, 3.18. Found: C, 26.56; H, 3.22. Heavy element ratios: Calcd: P/Pt, 1.00; P/Hg, 1.50; Cl/Hg, 1.00. Found: P/Pt, 0.98 ● 0.15; P/Hg, 1.65 ± 0.08; Cl/Hg, 1.16 ± 0.16.

$[\{HgBr_2\}_2\{Pt_3(\mu_2\text{-}CO)_3(P^iPr_3)_3\}]$ (11b). It was not isolated. Its structure and purity were confirmed by $^{31}P\{^1H\}$ NMR.

$[\{HgI_2\}_2\{Pt_3(\mu_2\text{-}CO)_3(P^iPr_3)_3\}]$ (11c). It was not isolated. Its structure and purity were confirmed by $^{31}P\{^1H\}$ NMR.

***cis*- and *trans*-$[PtI_2(CO)(PPh^iPr_2)_2]$ (16).** A solution of I_2 (0.061 g, 0.24 mmol) in CH_2Cl_2 (1 mL) was added to a solution of $[Pt_3(\mu_2\text{-}CO)_3(PPh^iPr_2)_3]$ (0.1 g, 0.08 mmol) in CH_2Cl_2. The mixture was stirred for 60 min and filtered over Celite. An orange powder was isolated after addition of hexane. Yield: 0.106 g (66%). The two isomers were not separated and their structures and relative amounts determined by NMR. ^{31}P NMR (cis isomer 98%): δ = 33.4 ppm, ^1J(Pt,P) = 2835 Hz; (trans isomer 2%): δ = 24.0 ppm, ^1J(Pt,P) = 2879 Hz. ^{195}Pt NMR (cis isomer): δ = −4980 ppm (d); (trans isomer): δ = −5540 ppm (d). IR: ν(CO): 2100 (s) cm^{-1}. This frequency is assignable to the cis complex. The corresponding band of the trans complex was not observed due to its low concentration. Anal. Calcd for $C_{13}H_{19}OI_2P_2Pt$: C, 23.24; H, 2.83; I, 37.85. Found: C, 23.22; H, 2.74; I, 37.62.

$[Pt_2I_2(CO)_2(PPh^iPr_2)]$ (17). A solution of I_2 (0.030 g, 0.12 mmol) in CH_2Cl_2 (1 mL) was added to a solution of $[Pt_3(\mu_2\text{-}CO)_3(PPh^iPr_2)_3]$ (0.1 g, 0.08 mmol) in CH_2Cl_2 (2 mL). A red crystalline powder was deposited after addition of hexane. Yield: 0.078 g (60%). ^{31}P NMR: δ = 58.9 ppm, ^1J(Pt,P) = 2604 Hz, ^2J(Pt,P) = 219 Hz, ^2J(P,P) = 164 Hz. ^{195}Pt NMR: δ = −4285 ppm. IR: ν(CO) 2085 (w), 2040 (s), 2020 (s) cm^{-1}. Anal. Calcd for $C_{26}H_{38}O_2I_2P_2Pt_2$: C, 28.69; H, 3.52; I, 23.34. Found: C, 29.17; H 3.69; I 24.08.

Determination and Refinement of the Structure of $\{9b\}_2 \cdot 6Me_2CO$. Crystals of $\{9b\}_2$ were obtained as described above.

The deep red crystals have prismatic habit and are unstable in the air due to loss of solvent. For the data collection a small prismatic crystal was sealed under nitrogen in a Lindemann glass capillary with the mother liquor. Space group and cell constants were determined on a Nonius CAD4 diffractometer which was subsequently used for the data collection. The symmetry of the crystal is trigonal and the systematic absences were consistent with space groups $R3c$ and $R\bar{3}c$. The centrosymmetric $R\bar{3}c$ space group was chosen as being appropriate for the symmetry of the cluster, thus allowing the minimum number of parameters in the refinement.

Cell constants were obtained by a least-squares fit of 25 high-angle reflections ($10° < \theta < 16°$) using the CAD4 centering routines[27] and are listed along with other crystallographic data in Table V and Supplementary Table S1. Three reflections were chosen as standards and measured every hour to check the stability of the crystal and of the experimental conditions; the crystal orientation was checked by measuring three standard reflections every 300.

Table VI. Table of Positional Parameters and Their Estimated Standard Deviations for $\{9b\}_2$

atom	x	y	z	B,[a] Å^2
Hg(1)	0.000	0.000	0.13387 (2)	6.21 (3)
Hg(2)	0.000	0.000	0.21574 (2)	4.50 (2)
Pt	0.06128 (4)	0.07964 (4)	0.17461 (1)	3.06 (2)
Br(1)	0.000	0.000	0.09124 (8)	13.7 (1)
Br(2)	−0.0302 (4)	0.0674 (4)	0.2498 (1)	10.4 (2)
P	0.1524 (3)	0.1964 (3)	0.17365 (9)	4.0 (2)
O	0.1820 (7)	0.0417 (7)	0.1742 (2)	5.5 (3)*
C	0.1166 (9)	0.0265 (8)	0.1744 (3)	3.3 (4)*
C(11)	0.184 (1)	0.233 (1)	0.1441 (3)	4.3 (5)*
C(12)	0.216 (1)	0.188 (1)	0.1328 (4)	4.7 (5)*
C(13)	0.240 (1)	0.221 (1)	0.1079 (4)	7.4 (7)*
C(14)	0.176 (1)	0.213 (1)	0.0945 (5)	8.0 (7)*
C(15)	0.148 (1)	0.259 (1)	0.1061 (4)	7.8 (7)*
C(16)	0.121 (1)	0.227 (1)	0.1310 (4)	6.4 (6)*
C(21)	0.234 (1)	0.208 (1)	0.1887 (4)	4.9 (5)*
C(22)	0.298 (1)	0.284 (1)	0.1867 (4)	8.5 (8)*
C(23)	0.366 (1)	0.291 (1)	0.1999 (5)	9.8 (9)*
C(24)	0.347 (2)	0.262 (1)	0.2232 (5)	10.1 (9)*
C(25)	0.285 (1)	0.190 (1)	0.2248 (5)	9.0 (8)*
C(26)	0.218 (1)	0.184 (1)	0.2131 (4)	6.7 (6)*
C(31)	0.130 (1)	0.262 (1)	0.1862 (3)	4.7 (5)*
C(32)	0.091 (1)	0.239 (1)	0.2071 (4)	5.3 (5)*
C(33)	0.069 (1)	0.289 (1)	0.2164 (5)	7.9 (7)*
C(34)	0.102 (1)	0.359 (1)	0.2093 (5)	11 (1)*
C(35)	0.138 (1)	0.380 (1)	0.1892 (5)	8.8 (8)*
C(36)	0.165 (1)	0.334 (1)	0.1791 (4)	8.8 (8)*
CS(1)	0.021 (3)	0.216 (3)	0.050 (1)	27 (2)*
CS(2)	0.109 (2)	0.216 (2)	0.0346 (7)	19 (2)*
CS(3)	0.039 (2)	0.179 (3)	0.0407 (9)	22 (2)*
CS(4)	0.035 (3)	0.116 (3)	0.033 (1)	24 (2)*

[a] Atoms with asterisks were refined isotropically. Anisotropically refined atoms are given in the form of the isotropic equivalent thermal parameter defined as: $(4/3)[a^2\beta(1,1) + b^2\beta(2,2) + c^2\beta(3,3) + ab(\cos\gamma)\beta(1,2) + ac(\cos\beta)\beta(1,3) + bc(\cos\alpha)\beta(2,3)]$.

Data were collected at variable scan speed to ensure constant statistical precision of the measured intensities. A total of 10349 reflections were measured and corrected for Lorentz and polarization factors and for decay (correction factors in the range 0.990–1.269). An empirical absorption correction was then applied using Ψ scans of four reflections at high χ angles ($\chi > 84°$). The corrected data were averaged to give a set of 3629 independent reflections of which 1294 were considered as observed having $F_o^2 \geq 3.0\sigma(F^2)$; an $F^2 = 0.0$ was given to those reflections having negative net intensities.

The structure was solved by Patterson and Fourier methods and refined using full matrix least squares, minimizing the function $(\sum w(|F_o| - 1/k|F_c|)^2)$. The scattering factors corrected for anomalous dispersion were taken from tabulated values.[28] Anisotropic temperature factors were used for the Pt, Hg, Br, and P atoms, while isotropic parameters were used for the remaining atoms. The contribution of the hydrogen atoms, held fixed in their calculated positions (C–H = 0.95 Å, B_{iso} = 3.0 Å) was taken into account but not refined.

Toward the end of the refinement a Fourier difference map revealed a clathrated acetone molecule; its contribution was taken into account during the refinement. All calculations were carried out using the Nonius SDP[27] package.

Final positional parameters are listed in Table VI.

Acknowledgment. K.-H.D. carried out the work during the tenure of a research fellowship from the Swiss National Research Council. A.A. acknowledges financial support from MURST. The Authors are indebted to Professor B. Magyar and Mr. B. Aeschlimann for the heavy metal analyses. J.F.M. and D.M.P.M. thank the SERC for financial support and Johnson-Matthey ple for a generous loan of platinum metals.

Supplementary Material Available: A table of full X-ray experimental data (Table S1), a table of anisotropic thermal displacements (Table S2), a table of calculated positions for the hydrogen atoms (Table S3), tables of extended list of bond lengths and angles (Table S4), and an ORTEP view of $\{9b\}_2$ with the numbering scheme (13 pages); a table of observed and calculated structure factors (Table S5) (9 pages). Ordering information is given on any current masthead page.

(27) *Enraf-Nonius Structure Determination Package SDP*; Enraf-Nonius: Delft, The Netherlands, 1987.

(28) *International Tables for X-ray Crystallography*; Kynoch Press: Birmingham, England, 1974; Vol. IV.